Controlled vapor crystal growth of $Na_4Ir_3O_8$: A three-dimensional quantum spin liquid candidate

Hong Zheng,[1,*] Junjie Zhang,[1,†] Constantinos C. Stoumpos,[2] Yang Ren,[3] Yu-Sheng Chen,[4] Rebecca Dally,[5,6] Stephen D. Wilson,[5] Zahirul Islam,[3] and J. F. Mitchell[1]

[1]*Materials Science Division, Argonne National Laboratory, Argonne, Illinois 60439, USA*
[2]*Department of Chemistry, Northwestern University, Evanston, Illinois 60208, USA*
[3]*X-ray Science Division, Advanced Photon Source, Argonne National Laboratory, Argonne, Illinois 60439, USA*
[4]*ChemMatCARS, The University of Chicago, Argonne, Illinois 60439, USA*
[5]*Materials Department, UC Santa Barbara, Santa Barbara, California 93106, USA*
[6]*Department of Physics, Boston College, Chestnut Hill, Massachusetts 02467, USA*

(Received 18 January 2018; published 24 April 2018)

We report the successful bulk single-crystal growth of the hyperkagome lattice iridate $Na_4Ir_3O_8$ (Na438) by vapor transport using a sealed aluminum oxide tube as a container. Crystals were characterized by magnetization, x-ray diffraction, and energy-dispersive x-ray measurements, confirming their identity and properties. Single-crystal x-ray diffraction experiments revealed superlattice peaks indexed on a propagation vector $q = (1/3,1/3,1/3)$ based on the cubic substructure with cell parameter $a = 8.986(1)$ Å. This superlattice is three-dimensional and fully coherent. Polarization analysis rules out spin and/or orbital order as the underlying origin of the modulation and points to long-range ordering of Na ions at the notionally disordered Na sites as a plausible origin for the observed superlattice.

DOI: 10.1103/PhysRevMaterials.2.043403

I. INTRODUCTION

Quantum spin liquid (QSL) is a state of quantum matter characterized by an ensemble of localized spin-1/2 units that are highly correlated yet do not order down to the lowest temperature [1–3]. Quantum spin liquids are prototypical examples of ground states with massive many-body entanglement, rendering these states distinct phases of matter with unique physical aspects such as nonlocal excitations and topological properties. To date, there are a few promising QSL candidates, including triangular-lattice κ-$(BEDT\text{-}TTF)_2Cu_2(CN)_3$ [4], $EtMe_3Sb[Pd(dmit)_2]_2$ [5], triangular-lattice $YbMgGaO_4$ [6–8], kagome lattice herbertsmithite $ZnCu_3(OH)_6Cl_2$ [9–11], honeycomb $RuCl_3$ [12–15], and hyperkagome lattice $Na_4Ir_3O_8$ (Na438) [16–31]. The last of these provides an example for which large spin-orbit coupling leads to a $J_{\text{eff}} = 1/2$ local at the Ir^{4+} sites, and it is the subject of this paper.

Na438 was first reported as an unidentified compound in the Na-Ir-O ternary system by McDaniel [32]. The crystal structure of $Na_4Ir_3O_8$ consists of a pyrochlore-like sublattice of metal ions, in which each tetrahedron of metals contains three Ir sites and one Na site [16]. Considering the Ir ions only, a corner-sharing network of triangles in three dimensions is formed, known as a "hyperkagome" lattice, with each Ir^{4+} site with a localized $J_{\text{eff}} = 1/2$ moment fourfold coordinated by nearest-neighbor Ir^{4+} ions. All the Ir sites and Ir-Ir bonds are symmetry-equivalent, causing a high degree of geometric frustration. Confirmation of the high degree of magnetic frustration in Na438 was initially suggested based on the measurement of a large Curie-Weiss temperature, $\Theta_{\text{CW}} = -650$ K, and spin freezing $T_{\text{f}} \sim 6$ K by Okamoto *et al.* [16]. More recent measurements by Dally *et al.* [33] have revealed an inhomogeneous distribution of spins occupying the entirety of the sample volume. They concluded that quasistatic, short-range spin correlations persist and differ from the nominally dynamic response of a quantum spin liquid [33,34].

Further progress in understanding the putative spin-liquid-like state in Na438 has been hindered by a lack of single crystals. Indeed, it is even challenging to obtain single-phase polycrystalline samples of Na438 due to the following three reasons: (i) The existence of competing phases such as Na_2IrO_3 and $Na_3Ir_3O_8$ (Na338), (ii) reactivity of Na with atmospheric moisture, and (iii) highly volatile starting materials such as Na_2CO_3 and IrO_2. Recently, Takayama *et al.* [34] have suggested that insulating Na438 crystals might be intergrown with semimetallic Na338 specimens grown from a flux, and that careful control of synthesis conditions could yield the desired Na438 phase in single-crystal form.

Herein we report the successful bulk single-crystal growth of Na438 by vapor transport in a hermetically sealed aluminum oxide tube, and we characterize its physical properties, including the spin freezing transition at $T_{\text{f}} \sim 6$ K. Unexpectedly, single-crystal x-ray diffraction revealed that the reported cubic structure ($P4_132$) is modulated with superlattice peaks characterized by a unique wave vector of $q = (1/3,1/3,1/3)$, which we suggest may arise from the ordering of sodium on the nominally disordered crystallographic sites.

II. EXPERIMENT

A. Crystal growth

Starting materials of Na_2CO_3 (99.99%, Alfa Aesar) and IrO_2 (99.99%, Alfa Aesar) were mixed thoroughly with the

*zheng@anl.gov
†Present address: Materials Science and Technology Division, Oak Ridge National Laboratory, Oak Ridge, TN 37831-6064, USA.

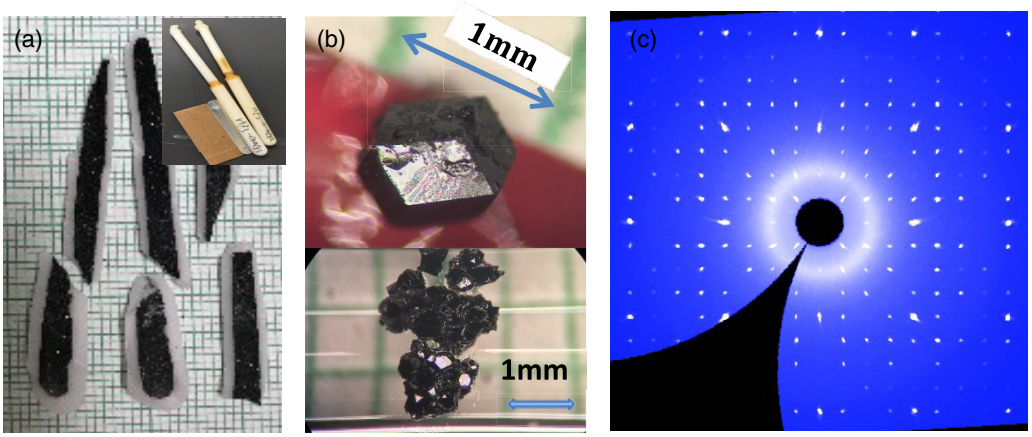

FIG. 1. (a) Crystals grown along the inside surface of the alumina tube (inset: sealed alumina tubes prior to crystal growth). (b) An as-grown $Na_4Ir_3O_8$ single crystal (top) and Na_2IrO_3 crystals (bottom). (c) $HK0$ plane of $Na_4Ir_3O_8$.

ratio of Na:Ir ranging from 4:3 to 4:1. The mixtures were calcined at 750 °C in air for 12 h, reground and pressed into pellets, and then sintered at 900 °C in air for 12 h. Each mixture ($\sim$0.4g) was placed into an alumina tube with 6 mm ID. The alumina tube was sealed using an optical floating zone furnace (SciDre GmbH Model HKZ). Specifically, the aluminum oxide tube was affixed to the bottom shaft and a solid Al_2O_3 rod was affixed on the top shaft. The system was evacuated to 10^{-3} mbar, and then oxygen was backfilled to 5 bar and then reduced to 1 bar total pressure. This process was repeated twice. Finally, the tube was sealed under 1 bar pressure of O_2. In a typical growth experiment, the sealed tube was placed vertically in a box furnace and heated to 1190 °C at a rate of 100 °C/h, held at this temperature for 72 h, and then cooled down to 1080 °C at a rate of 2 °C/h, followed by cooling down to room temperature at a rate of 100 °C/h. Black, rhombic dodecahedral single crystals with dimensions up to 1mm^3 were obtained on the side of the alumina tube, as shown in Fig. 1, along with platelike Na_2IrO_3 single crystals as a byproduct. Due to the known reactivity of alkali-metal-containing transition-metal oxides to air, all crystals were manipulated and stored in a nitrogen-filled glove box to protect them from decomposition between measurements.

B. Powder x-ray diffraction

Powder x-ray diffraction data were collected at room temperature on pulverized single crystals using a PANalytical X'Pert Pro powder diffractometer with Cu $K\alpha$ radiation (λ = 1.5418 Å) in the range 5°–80°2θ.

C. Elemental analysis

The chemical composition of the single crystals was determined using a Hitachi S4700 scanning electron microscope (SEM) with an energy-dispersive x-ray spectrometer (EDS).

D. Single-crystal x-ray diffraction

Single-crystal x-ray diffraction data at 100 K were collected with a Bruker APEX2 diffractometer (λ = 0.71073 Å). Calculations were performed using the APEX2 crystallographic software package [35]. The structure was refined using the model from Okamoto *et al.* [16] as a starting point with full matrix least-squares methods on F^2. Iridium atoms were modeled using anisotropic ADPs, and the refinements converged for $I > 2\sigma(I)$. Single-crystal x-ray diffraction at room temperature was carried out on a STOE IPDS 2 T diffractometer. Data reduction and an absorption correction were performed with the software X-Area [36]. Single-crystal x-ray diffraction data were also collected with an APEX2 area detector using synchrotron radiation (λ = 0.41328 Å) at Beamline 15-ID-B at the Advanced Photon Source, Argonne National Laboratory. A single crystal of Na438 with dimensions of approximately 5 μm on an edge was attached to the tip of a glass fiber and mounted on the goniometer. Indexing was performed using Bruker APEX2 software [35]. Data integration and cell refinement were performed using SAINT [35]. A stoichiometric (as adjudged by magnetization) Na438 single-crystal specimen with a well-defined pristine surface was also studied on the 6-ID-B,C beamline of the Advanced Photon Source using high-resolution diffraction in reflection geometry and resonant-scattering techniques. A Si (111) double-bounce monochromator was used to select a photon energy with an $\sim$0.01% bandwidth. For the diffraction experiment, photon energy was tuned near the Ir L_3 edge (λ = 1.1055 A, 11.215 keV). The beam was focused in the vertical plane using a bent ultralow expansion mirror. A point detector (Na I scintillator) behind a PG(008) analyzer was used to measure diffracted intensity of charge Bragg peaks and to perform polarization analyses. The incident beam intensity was measured with a helium gas filled ion chamber. The sample was cooled to below 2 K using a cryostat with a Joule-Thompson stage. While multiple grains were detected in the sample, measurements were carried out on the strongest grain with mosaic <0.1° and a cell parameter of 8.972 Å. Incident flux was reduced by orders of magnitude to avoid beam heating above 6 K.

E. Magnetic susceptibility

Magnetic susceptibility measurements were performed on single crystals using a Quantum Design MPMS-3 SQUID magnetometer. The crystal shown in Fig. 1(a) was attached to a quartz rod using a minimum amount of Apiezon grease. Zero-field-cooled (ZFC) and field-cooled (FC) data were collected

under a magnetic field of 0.2 T. The sample was cooled in zero field to 2 K at a rate of 35 K/min, and dc magnetization was recorded while warming (1 K/min from 2 to 20 K and 2 K/min from 20 to 60 K, then 5 K/min from 60 to 300 K), then the sample was cooled with field at 35 K/min to 2 K, and then dc magnetization data were collected on warming using the same protocol as ZFC.

III. RESULTS AND DISCUSSION

A. Crystal growth

Single-crystal growth of sodium-iridium oxide compounds is challenging due to the volatile nature of the components. In particular, IrO_2 reacts with O_2 above 1020 °C to form the volatile phase IrO_3. Likewise, the high vapor pressure of alkali metals such as Na above 1000 °C complicates growth in an open system. To accommodate this volatility, crystals of iridates have typically been grown by the flux method below 1000 °C. For instance, Na_2IrO_3 single crystals have been grown from Na_2CO_3 flux at 950 °C [37]. On the other hand, it would be desirable to take advantage of this volatility to grow crystals in a closed system by vapor transport. Due to the reactivity between sodium and fused silica, sealed tubes made of this material are not an option. Therefore, we selected a sealed aluminum oxide (998 alumina) tube to perform the vapor crystal growth. The advantages of a sealed alumina tube are as follows: (i) the sealed system can contain the vapor inside of an alumina tube without losing any material during crystal growth, (ii) temperatures can be reached much higher than for a silica tube, and (iii) there is no or very little reaction between aluminum oxide and Na_2IrO_3, Na_2CO_3, and IrO_2 in the working temperature range.

Figure 1(a) shows the single crystals grown on the entire side of the aluminum oxide tube, well separated from the starting material as expected from a vapor growth process. Typically, two kinds of single crystals are found inside the aluminum oxide tube that can be easily separated based on their morphology. As shown in Fig. 1(b), one kind (found in sizes up to 1 mm on an edge) shows a rhombic dodecahedral shape [upper crystal of Fig. 1(b)], the other type evidences a hexagonal, platelike shape [lower crystals of Fig. 1(b)]. X-ray diffraction unequivocally identifies these platelike crystals as Na_2IrO_3. Figure 1(c) presents the $(H\,K\,0)$ diffraction plane of one of the dodecahedral crystals (confirmed to be Na438; see below) measured on a laboratory diffractometer [36], attesting to the single crystallinity of the specimen. Furthermore, powder x-ray diffraction of pulverized dodecahedral crystals matches well with the pattern reported by Okamoto *et al.* [16] and Dally *et al.* [33] We note here that the latter authors have shown that the powder diffraction pattern of Na438 is nearly indistinguishable from the related compound $Na_3Ir_3O_8$ (Na338), which is a B-site ordered spinel, $Na(Na_{1/4}Ir_{3/4})_2O_4$, shown to be a nonmagnetic semimetal by Takayama *et al.* [34]. In particular, Na338 and Na438 share a common space group and Ir hyperkagome sublattice, meaning these two compounds exhibit only subtle differences in x-ray intensities [34]. Fortunately, Dally *et al.* [33,38] have shown that magnetic susceptibility provides a definitive means to distinguish between Na338 and Na438, the latter exhibiting a cusp near 6 K and the former an essentially temperature-independent paramagnetism. Using this magnetic diagnostic, among the rhombic dodecahedral crystals harvested from several batches, both Na338 and Na438 can be found as competing phases. Thus, in the process of optimizing growth and ultimately characterizing crystal properties, individual single crystals must be screened based on their magnetic response to unambiguously identify Na438 specimens. We have followed this approach throughout this study.

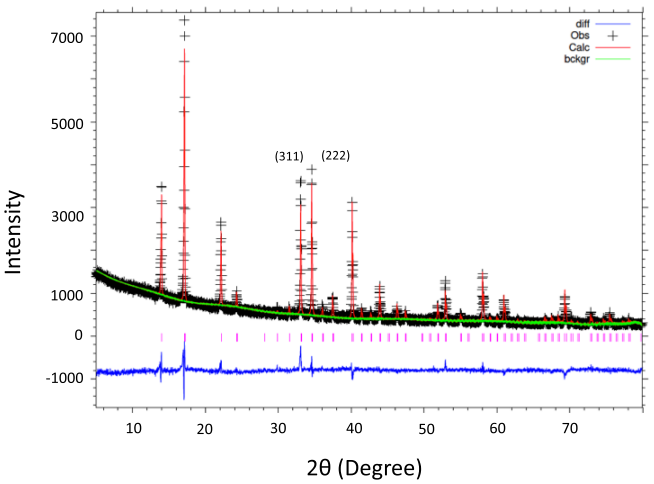

FIG. 2. Rietveld refinement of laboratory powder x-ray diffraction pattern of pulverized Na438 single crystals. Crosses, data; solid green line, calculated fit; tick marks, expected reflection positions; solid blue line, difference $I_{obs} - I_{calc}$.

Figure 2 shows Rietveld refinement of a laboratory powder x-ray diffraction pattern of pulverized single crystals identified by magnetic susceptibility to be Na438. We find good agreement between the model of Okamoto *et al.* [16] and our data, and the refined lattice parameter in space group $P4_132$ compares favorably to the value 8.985 Å reported by these authors. Note specifically the intensity ratio of the (311) and (222) reflections, which Dally *et al.* [33] have offered as a diagnostic for separating Na438 from Na338 by x-ray diffraction.

To optimize the growth conditions of Na438 empirically, we explored both temperature and starting composition as variables. Due to the phase competition described above and the similar appearance of Na438 and Na338 crystals, we typically screened more than a dozen rhombic dodecahedral crystals out of each batch using magnetic susceptibility. Comments on phase predominance are based on this survey, which is perforce semiquantitative. With this caveat, we were able to establish certain trends in the dependence of outcome on the growth parameters. We started with a 2:1 molar ratio of Na:Ir, from which we fortuitously first identified the appearance of 438 crystals at 1080 °C. The yield of Na438 was favored by increasing temperature at this 2:1 Na/Ir ratio and was optimized at 1190 °C in our experiments. We began to see IrO_2 and Ir metal at 1250 °C. We then explored the effect of the Na:Ir ratio at the optimized soaking temperature, 1190 °C. Specifically, we tested three different ratios of Na:Ir in the starting materials: 4:3, 2:1, and 4:1. Of these, 2:1 was found best for growing Na438 from vapor. To summarize our empirical findings: Na438 is favored in the range 1080–1200 °C using a 2:1 ratio of Na:Ir in the starting materials. Above 1080 °C, Na338

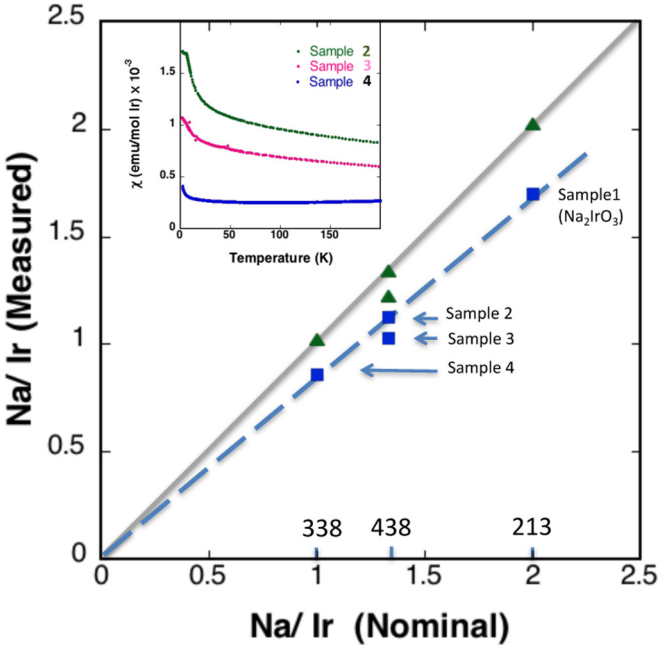

FIG. 3. EDX measurement. Squares show as-measured composition, and green triangles are the Na_2IrO_3, $Na_{4-x}Ir_3O_8$, and $Na_3Ir_3O_8$ compositions after correction. Inset: magnetic susceptibility measured on the same samples.

begins to predominate when the Na:Ir ratio exceeds 2:1, a counterintuitive result. Na_2IrO_3 is found in all growths as a competing phase.

B. Crystal stoichiometry

Because of the possibility of Na nonstoichiometry reported in ceramic samples [33], the chemical composition of the single crystals was studied via energy-dispersive x-ray spectroscopy (EDX). Rhombic dodecahedral single-crystal samples (denoted 2, 3, and 4) were selected by magnetization measurements, which showed significant dispersion (see the inset of Fig. 3). Based on the form of these magnetic data and a comparison to the data of Dally *et al.* [33], we expect sample 2 to be Na438, sample 4 to be Na338 and sample 3 to interpolate between Na438 and Na338, indicating the possibility of at least a partial $Na_{4-x}Ir_3O_8$ solid solution as reported by Singh [17] or a phase separation.

EDX confirms this assignment. All samples were polished and covered by 20 nm of gold before EDX measurement. We used a single crystal of Na213 (grown using Na_2CO_3 as a flux and characterized via magnetization and single-crystal diffraction) as an external reference since it is considered a line compound [37]. No aluminum signal was found for any measured sample. We show the results of the EDX measurements in Fig. 3, where the horizontal axis is the nominal Na:Ir ratio, the measured value is plotted as blue squares, and the solid gray line represents perfect agreement between the nominal and measured ratio. The measured Na:Ir ratio of samples 1, 2, and 4 varies linearly with the nominal values (dashed blue line); however, a slope deviating from unity reveals a systematic error in the measured values based on the internal reference used by the instrument. Using the Na213 data as an external reference,

TABLE I. Sample composition measured by EDX.

Sample no.	Nominal composition	As-measured	Normalized to Na_2IrO_3
1	Na_2IrO_3	$Na_{1.7}IrO_3$	Na_2IrO_3
2	$Na_4Ir_3O_8$	$Na_{3.4}Ir_3O_8$	$Na_{3.99}Ir_3O_8$
3	$Na_4Ir_3O_8$	$Na_{3.1}Ir_3O_8$	$Na_{3.61}Ir_3O_8$
4	$Na_3Ir_3O_8$	$Na_{2.6}Ir_3O_8$	$Na_{3.05}Ir_3O_8$

this systematic error can be corrected by applying a multiplier of 1.19 to all the measured data. This correction brings samples 1, 2, and 4 onto the ideal composition line (green triangles) with 2:1, 4:3, and 1:1 compositions, respectively, in agreement with expectations from the magnetization. The corrected Na:Ir ratio found for sample 3 lies off the ideal composition line and is thus determined to be Na-deficient. Table I shows the Na:Ir ratios both before and after correction for all samples 1–4.

C. Magnetic properties

The temperature-dependent magnetic susceptibility of several other samples grown under optimized conditions is plotted in Fig. 4. Based on the EDX results above, we assert that the Na content is decreasing in these samples in the order $a > b > c > d$. Sample a shows a clear signature of an ordering process at 6 K (shown more clearly in the inset), which Dally *et al.* have attributed to freezing of spins based on μSR data [33]. A similar interpretation has been offered by Shockley *et al.* from NMR studies [39]. Curves *b*-*d* show that although the 6 K spin-freezing temperature remains reasonably constant, this feature gradually washes out as Na content decreases, tending toward a temperature-independent magnetization attributed to the Na338 phase [33]. One interpretation of this behavior is a phase separation, in which nominal $Na_{4-x}Ir_3O_8$ separates into end-member phases, $Na_4Ir_3O_8$ and $Na_3Ir_3O_8$. A Curie-Weiss fit to the data between 100 and 300 K yields $\Theta_W = -472, -475$, and -545 K for samples a, b, and c, respectively,

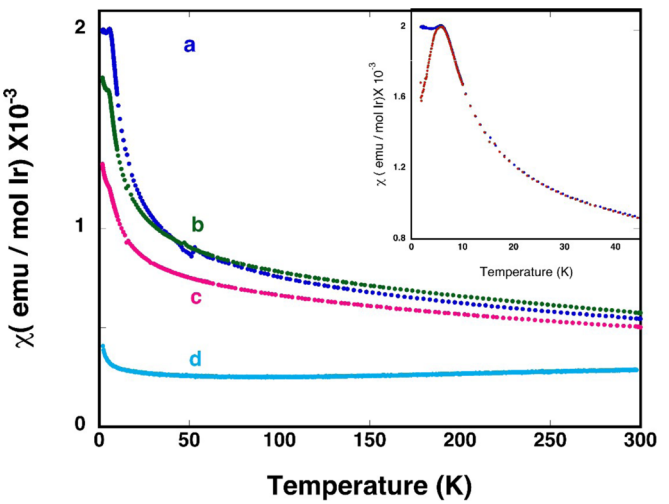

FIG. 4. Magnetic susceptibility measured on warming at 0.2 T after field cooling (inset: low-temperature region of curve a).

TABLE II. Crystal data and structure refinement for $Na_4Ir_3O_8$ based on Ref. [16].

Empirical formula	$Na_4Ir_3O_8$
Formula weight	796.56
Temperature	100(2) K
Wavelength	0.71073 Å
Crystal system, space group	Cubic, $P4_132$
Unit-cell dimensions	$a = 8.982(2)$ Å
Volume	724.7(5) $Å^3$
Z	4
Density (calculated)	7.301 Mg/m^3
Absorption coefficient	55.208 mm^{-1}
$F(000)$	1356
θ range for data collection	3.207°–31.155°
Index ranges	$-12 \leqslant h \leqslant 12, -12 \leqslant k \leqslant 13, -12 \leqslant l \leqslant 12$
Reflections collected	5799
Independent reflections	399[R(int) = 0.0842]
Completeness to $\theta = 25.242°$	100.0%
Refinement method	Full-matrix least-squares on F2
Data / restraints / parameters	399 / 0 / 17
Goodness-of-fit on F^2	1.224
Final R indices [$I > 2\sigma(I)$]	$R_1 = 0.0391, wR_2 = 0.0895$
R indices (all data)	$R_1 = 0.0530, wR_2 = 0.0956$
Absolute structure parameter	0.7(3)
Largest diff. peak and hole	8.138 and −4.218 e $Å^{-3}$

with corresponding effective local moments of 1.82 μ_B/Ir, 1.88 μ_B/Ir, and 1.84μ_B/Ir. These values are close to the 1.73μ_B/Ir expected for a $J_{\text{eff}} = 1/2$ system.

D. Crystal structure determination

The structure of $Na_4Ir_3O_8$ was reported by Okamoto *et al.* [16] from Rietveld refinement of powder x-ray diffraction.

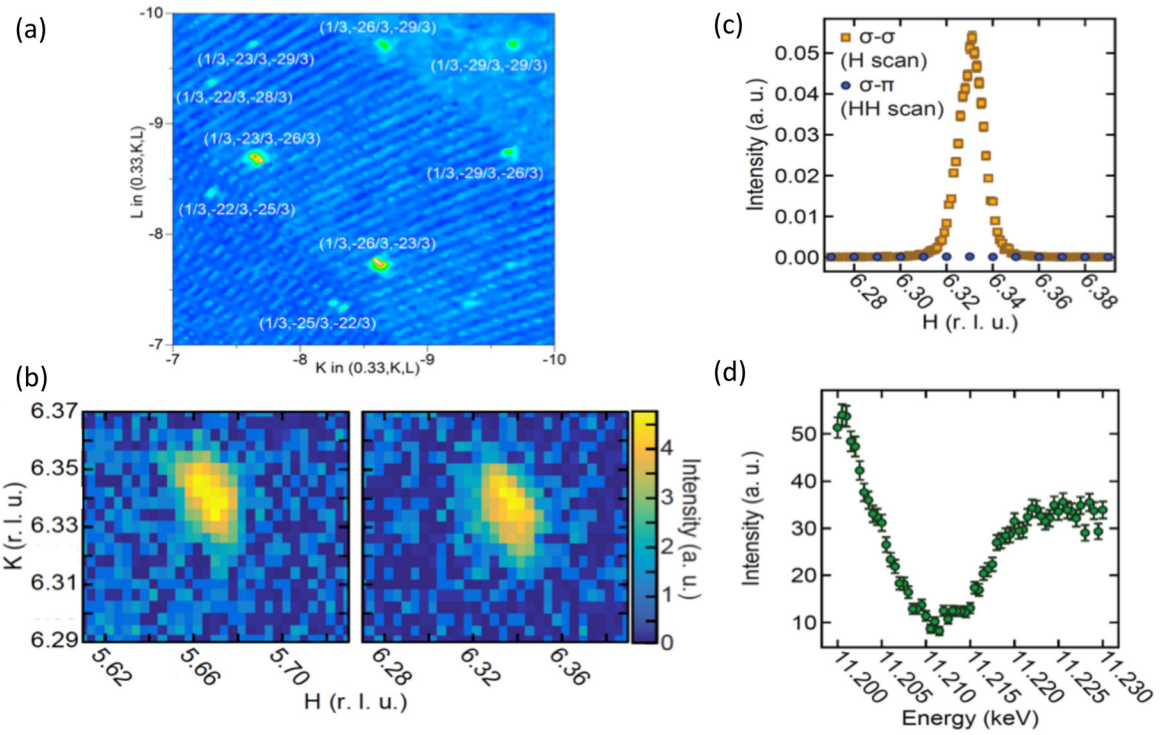

FIG. 5. (a) Section of the (1/3,K, L) plane showing several superlattice reflections at 200 K. (b) A representative (H, K) map of scattering about the (1/3,1/3,1/3) satellite peaks at the (6,6,1) zone center. The L value is 1.33. (c) H scan through the (6.33,6.33,1.33) satellite in both the σ-σ and σ-π scattering channels. (d) Energy scan conducted while sittingσ at Q = (6.33,6.33,1.33). Parts (b)–(d) were collected at 1.8 K.

They based their model on the known structure of $Na_4Sn_3O_8$ [40], assuming that two Na ions, Na2 and Na3, are located in octahedral sites (Wyckoff positions 4*a* and 12*d*, respectively), both fully disordered with 75% occupation. Using this structure as a starting point, we refined the structure of our single crystal of 438 (selected based on magnetization) on lab-based x-ray diffraction data collected at 100 K (Tables II and III). Table II lists the refinement results with a reasonable, but not exceptional, *R* factor of 3.91%. In the refinement process, we found a strong residual electron density peak very close to Na2 (1.935 Å) and Na3 (1.956 Å), leading us to question the appropriateness of the $Na_4Sn_3O_8$ model for $Na_4Ir_3O_8$.

To further explore the validity of the $Na_4Sn_3O_8$ model for $Na_4Ir_3O_8$, we performed high-energy XRD measurements at beamline 15-ID-B of the Advanced Photon Source at Argonne National Laboratory. We measured small ($\sim 130\,\mu m^3$) single-crystal samples (with EDX-determined $Na_{3.99}Ir_3O_8$ and $Na_3Ir_3O_8$) at 200 K. The diffraction pattern can be indexed using a cubic lattice $a = 8.968(1)$ Å, but structural refinement encounters the same problem as observed in the lab x-ray. In fact, examination of the synchrotron data [Fig. 5(a)] revealed previously unidentified superlattice peaks that can be indexed with the wave vector (1/3,1/3,1/3) based on the cubic subcell.

To explore the structure below the spin-freezing temperature, we have carried out high-resolution diffraction using both resonant and nonresonant scattering techniques on beamline 6-ID-B & C. Well-defined Bragg peaks consistent with the refinements presented above were observed. Extensive scans along several high-symmetry directions away from these Bragg peaks confirmed the presence of the $q = (1/3,1/3,1/3)$ superstructure. Two representative superlattice reflections are shown in Fig. 5(b), from which we find that the superstructure is fully coherent and three-dimensionally ordered. The data in Fig. 5(b) were collected using 11.2 KeV (1.107 Å) below the absorption edge to minimize absorption and beam heating. Polarization analyses (11.215 KeV) at base temperature [Fig. 5(c)] showed that the superstructure peaks associated with (1/3,1/3,1/3)-type peaks appear only in the σ-σ charge-scattering channel, while energy scans through the Ir L_3 edge [Fig. 5(d)] were consistent with only absorption without any resonant enhancements. These observations indicate that the satellite is structural in origin with no obvious spin and/or orbital ordering component.

The discovery of this weak, albeit fully coherent, structural modulation offers a potential explanation for why our refinement captured the average structure well yet showed some strong residual electron density at Na sites. Although the detailed nature of the superstructure will require further investigation, the possibility of long-range Na-ion ordering across the nominally disordered sites [Na(2) and Na(3)] is consistent with such behavior and is likely the origin of the superstructure. Consistent with this explanation, the (1/3,1/3,1/3) superlattice peaks were completely absent from a crystal of semimetallic Na338 with its fully ordered Na sublattice.

TABLE III. Atomic coordinates and equivalent isotropic displacement parameters. U_{eq} is defined as one-third of the trace of the orthogonalized U_{ij} tensor. ESDs are given in parentheses.

	x	*y*	*z*	U_{eq}	Occupancy
Ir(1)	0.6153(1)	0.8653(1)	0.6250	0.005(1)	1
O(1)	0.1146(11)	0.1146(11)	0.1146(11)	0.007(3)	1
O(2)	0.1337(13)	0.9026(13)	0.9111(13)	0.010(2)	1
Na(1)	0.8750	0.8750	0.8750	0.003(3)	1
Na(2)	0.3750	0.3750	0.3750	0.037(7)	0.75
Na(3)	0.3605(12)	0.6105(12)	0.6250	0.022(4)	0.75

IV. CONCLUSIONS

Single crystals of Na438 with dimensions up to $1mm^3$ have been grown using natural vapor transport in sealed alumina tubes. The as-grown crystals show a spin-freezing transition at $T \sim 6$ K that gradually evolves with decreasing Na content, $Na_{4-x}Ir_3O_8$. Our method also provided Na338 crystals that show paramagnetic semimetallic behavior in accord with the literature [34]. Synchrotron x-ray single-crystal diffraction data measured on Na438 revealed a fully coherent and three-dimensional superlattice indexed by the propagation vector $q = (1/3,1/3,1/3)$ based on the cubic subcell. This latter finding indicates that the existing structural models for Na438 in the literature are incomplete and further may impact interpretation of data and theoretical modeling of this frustrated $J_{eff} = 1/2$ system. Finally, the vapor growth method described here offers an alternative growth approach for those materials that cannot be grown in a sealed fused silica tube due to the limit of either temperature or alkali-metal attack.

ACKNOWLEDGMENTS

Work in the Materials Science Division at Argonne National Laboratory (crystal growth, x-ray analysis and magnetic characterization) was sponsored by the US Department of Energy Office of Science, Basic Energy Sciences, Materials Science and Engineering Division. This research has been supported in part by ORNL Post Doctoral Development Fund by UT-Battelle, LLC under Contract No. DE-AC05-00OR22725 with the US Department of Energy. Work at UCSB (analysis of resonant scattering synchrotron data) was supported by NSF Award No. DMR-1505549. ChemMatCARS Sector 15 is principally supported by the Divisions of Chemistry (CHE) and Materials Research (DMR), National Science Foundation, under Grant No. NSF/CHE-1346572. Use of the Advanced Photon Source, a US Department of Energy Office of Science User Facility operated for the Department of Energy Office of Science by Argonne National Laboratory under Contract No. DE-AC02-06CH11357.

[1] Y. Zhou, K. Kanoda, and T.-K. Ng, Rev. Mod. Phys. **89**, 025003 (2017).
[2] L. Savary and L. Balents, Rep. Prog. Phys. **80**, 016502 (2017).
[3] M. R. Norman, Rev. Mod. Phys. **88**, 041002 (2016).

[4] Y. Shimizu, K. Miyagawa, K. Kanoda, M. Maesato, and G. Saito, Phys. Rev. Lett. **91**, 107001 (2003).

[5] S. Yamashita, T. Yamamoto, Y. Nakazawa, M. Tamura, and R. Kato, Nat. Commun. **2**, 275 (2011).

[6] J. A. M. Paddison, M. Daum, Z. Dun, G. Ehlers, Y. Liu, M. B. Stone, H. Zhou, and M. Mourigal, Nat. Phys. **13**, 117 (2017).

[7] Y. Shen, Y.-D. Li, H. Wo, Y. Li, S. Shen, B. Pan, Q. Wang, H. C. Walker, P. Steffens, M. Boehm, Y. Hao, D. L. Quintero-Castro, L. W. Harriger, M. D. Frontzek, L. Hao, S. Meng, Q. Zhang, G. Chen, and J. Zhao, Nature (London) **540**, 559 (2016).

[8] Y. Li, G. Chen, W. Tong, L. Pi, J. Liu, Z. Yang, X. Wang, and Q. Zhang, Phys. Rev. Lett. **115**, 167203 (2015).

[9] M. P. Shores, E. A. Nytko, B. M. Bartlett, and D. G. Nocera, J. Am. Chem. Soc. **127**, 13462 (2005).

[10] T.-H. Han, J. S. Helton, S. Chu, D. G. Nocera, J. A. Rodriguez-Rivera, C. Broholm, and Y. S. Lee, Nature (London) **492**, 406 (2012).

[11] M. Fu, T. Imai, T.-H. Han, and Y. S. Lee, Science **350**, 655 (2015).

[12] J. C. Zheng, K. J. Ran, T. R. Li, J. H. Wang, P. S. Wang, B. Liu, Z. X. Liu, B. Normand, J. S. Wen, and W. Q. Yu, Phys. Rev. Lett. **119**, 227208 (2017).

[13] A. Banerjee, J. Q. Yan, J. Knolle, C. A. Bridges, M. B. Stone, M. D. Lumsden, D. G. Mandrus, D. A. Tennant, R. Moessner, and S. E. Nagler, Science **356**, 1055 (2017).

[14] S. H. Baek, S. H. Do, K. Y. Choi, Y. S. Kwon, A. U. B. Wolter, S. Nishimoto, J. van den Brink, and B. Buchner, Phys. Rev. Lett. **119**, 037201 (2017).

[15] A. Banerjee, C. A. Bridges, J. Q. Yan, A. A. Aczel, L. Li, M. B. Stone, G. E. Granroth, M. D. Lumsden, Y. Yiu, J. Knolle, S. Bhattacharjee, D. L. Kovrizhin, R. Moessner, D. A. Tennant, D. G. Mandrus, and S. E. Nagler, Nat. Mater. **15**, 733 (2016).

[16] Y. Okamoto, M. Nohara, H. Aruga-Katori, and H. Takagi, Phys. Rev. Lett. **99**, 137207 (2007).

[17] Y. Singh, Y. Tokiwa, J. Dong, and P. Gegenwart, Phys. Rev. B **88**, 220413 (2013).

[18] J. G. Rau, E. K.-H. Lee, and H.-Y. Kee, Annu. Rev. Condens. Matter Phys. **7**, 195 (2016).

[19] B. Huang, Y. B. Kim, and Y.-M. Lu, Phys. Rev. B **95**, 054404 (2017).

[20] T. Mizoguchi, K. Hwang, E. K.-H. Lee, and Y. B. Kim, Phys. Rev. B **94**, 064416 (2016).

[21] G. Chen and Y. B. Kim, Phys. Rev. B **87**, 165120 (2013).

[22] D. Podolsky and Y. B. Kim, Phys. Rev. B **83**, 054401 (2011).

[23] M. R. Norman and T. Micklitz, Phys. Rev. B **81**, 024428 (2010).

[24] T. Micklitz and M. R. Norman, Phys. Rev. B **81**, 174417 (2010).

[25] E. J. Bergholtz, A. M. Läuchli, and R. Moessner, Phys. Rev. Lett. **105**, 237202 (2010).

[26] D. Podolsky, A. Paramekanti, Y. B. Kim, and T. Senthil, Phys. Rev. Lett. **102**, 186401 (2009).

[27] Y. Zhou, P. A. Lee, T.-K. Ng, and F.-C. Zhang, Phys. Rev. Lett. **101**, 197201 (2008).

[28] M. J. Lawler, A. Paramekanti, Y. B. Kim, and L. Balents, Phys. Rev. Lett. **101**, 197202 (2008).

[29] M. J. Lawler, H.-Y. Kee, Y. B. Kim, and A. Vishwanath, Phys. Rev. Lett. **100**, 227201 (2008).

[30] G. Chen and L. Balents, Phys. Rev. B **78**, 094403 (2008).

[31] S. N. Gupta, P. V. Sriluckshmy, A. Balodhi, D. V. S. Muthu, S. R. Hassan, Y. Singh, T. V. Ramakrishnan, and A. K. Sood, Phys. Rev. B **94**, 155153 (2016).

[32] C. L. McDaniel, J. Solid State Chem. **9**, 139 (1974).

[33] R. Dally, T. Hogan, A. Amato, H. Luetkens, C. Baines, J. Rodriguez-Rivera, M. J. Graf, and S. D. Wilson, Phys. Rev. Lett. **113**, 247601 (2014).

[34] T. Takayama, A. Yaresko, A. Matsumoto, J. Nuss, K. Ishii, M. Yoshida, J. Mizuki, and H. Takagi, Sci. Rep. **4**, 6818 (2014).

[35] Bruker AXS, Inc. APEX2. Bruker AXS Inc., Madison, WI, USA (2014).

[36] Stoe & Cie. X-AREA/X-RED/X-SHAPE. Stoe & Cie, Darmstadt, Germany (2002).

[37] S. H. Chun, J.-W. Kim, J. Kim, H. Zheng, C. C. Stoumpos, C. D. Malliakas, J. F. Mitchell, K. Mehlawat, Y. Singh, Y. Choi, T. Gog, A. Al-Zein, M. M. Sala, M. Krisch, J. Chaloupka, G. Jackeli, G. Khaliullin, and B. J. Kim, Nat. Phys. **11**, 462 (2015).

[38] A. Balodhi, A. Thamizhavel, and Y. Singh, Phys. Rev. B **91**, 224409 (2015).

[39] A. C. Shockley, F. Bert, J. C. Orain, Y. Okamoto, and P. Mendels, Phys. Rev. Lett. **115**, 047201 (2015).

[40] M. Iwasaki, H. Takizawa, K. Uheda, and T. Endo, J. Mater. Chem. **12**, 1068 (2002).